Research Article

ADVANCED PHOTONICS

On-the-fly precision spectroscopy with a dual-modulated tunable diode laser and Hz-level referencing to a cavity

Shuangyou Zhang,[a] Toby Bi,[a,b] and Pascal Del'Haye[a,b,*]
[a]Max Planck Institute for the Science of Light, Erlangen, Germany
[b]Friedrich-Alexander Universität Erlangen-Nürnberg, Department of Physics, Erlangen, Germany

Abstract. Advances in laser spectroscopy have enabled many scientific breakthroughs in physics, chemistry, biology, and astronomy. Optical frequency combs pushed measurement limits with ultrahigh-frequency accuracy and fast-measurement speed, while tunable-diode-laser spectroscopy is used in scenarios that require high power and continuous spectral coverage. Despite these advantages of tunable-diode-laser spectroscopy, it is challenging to precisely determine the instantaneous laser frequency because of fluctuations in the scan speed. Here, we demonstrate a simple spectroscopy scheme with a frequency-modulated diode laser that references the laser on-the-fly to a fiber cavity. The fiber cavity's free spectral range is on-the-fly calibrated with sub-10-Hz frequency precision. We achieve a relative precision of the laser frequency of 2×10^{-8} for an 11-THz frequency range at a measurement speed of 1 THz/s. This is an improvement of more than 2 orders of magnitude compared to existing diode-laser-spectroscopy methods. Our scheme provides precise frequency calibration markers, while simultaneously tracking the instantaneous scan speed of the laser. We demonstrate the versatility of our method through various applications, including dispersion measurement of a fiber, ultrahigh-Q microresonators, and spectroscopy of a hydrogen fluoride gas cell. The simplicity, robustness, and low cost of this spectroscopy scheme are valuable for out-of-the-lab applications like lidar and environmental monitoring.

Keywords: tunable laser spectroscopy; radio-frequency modulation; integrated photonics; gas spectroscopy; frequency comb.

Received Jul. 16, 2024; accepted for publication Jul. 18, 2024; published online Aug. 9, 2024.

[DOI: 10.1117/1.AP.6.4.046003]

1 Introduction

Since the first demonstration of the laser in the 1960s, laser spectroscopy has been an ultimate tool for studies on detailed structures and dynamics in atoms and molecules,[1] further boosted by the progress of tunable continuous-wave (CW) lasers and optical frequency combs.[2–4] In particular, the development of optical frequency combs enabled frequency metrology with unprecedented precision of up to 18 digits,[5] leading to a rapidly growing number of applications.[6,7] In addition to "single-frequency" metrology, optical frequency combs have also been utilized for high-precision and high-speed broadband spectroscopy, benefiting from their unique combination of large bandwidth and high spectral resolution. Within the last two decades, a diverse set of spectroscopic methods based on optical frequency combs has been developed: for example, direct frequency comb spectroscopy,[8] dual-comb spectroscopy,[9,10] two-dimensional optical frequency "brushes,"[11] Fourier transform spectroscopy,[12] and a Vernier spectrometer.[13] A disadvantage of spectroscopy with frequency combs is the low power per comb mode, which makes sensing of trace gas samples challenging. In addition, most combs exhibit a significant variation of power in different spectral regions, which can hinder broadband spectroscopy.[7] As a further complication, high-precision measurements based on optical frequency combs often require comb sources with long-term coherence, which requires sophisticated servo loops.[6]

Tunable CW lasers are widely used for highly sensitive molecular spectroscopy, gas sensing, lidar, and optical vector network analyzers for characterization of optical systems and

*Address all correspondence to Pascal Del'Haye, pascal.delhaye@mpl.mpg.de

components.[14,15] In spectroscopy, tunable lasers can achieve high signal-to-noise ratios (SNRs) because of their high photon flux and have advantages of long interaction paths and frequency agility. However, the system performances (frequency precision and resolution) are usually limited by fluctuations of the laser frequency scan speed. To calibrate a nonlinear scanning of the laser frequency, different methods have been developed using interferometric approaches,[16] wavelength meters,[17] optical channel estimation,[18] single-sideband modulation,[14,19] and optical frequency combs.[20,21] In particular, frequency-comb-calibrated diode laser spectroscopy was demonstrated by combining the accuracy of a frequency comb with the tunability and high power of a tunable laser, enabling broadband spectroscopy with bandwidth >4 THz, scanning speed >1 THz/s, and megahertz-level resolution.[20] This method has wide applications in different areas, such as dispersion characterization of microresonators,[20,22,23] absolute distance measurements,[24,25] precision characterization of dynamic CW lasers,[26,27] three-dimensional imaging,[28] molecular spectroscopy,[29] and calibration of astrophysical spectra.[30] However, to generate frequency calibration markers with a high SNR, this method requires a reference frequency comb with a flat optical spectrum and constant polarization over a wide spectrum. However, it is in particular challenging to measure very narrow spectral features across a broad spectral range with high power and high SNR. In addition, most frequency-comb-based applications are demonstrated in laboratory settings due to the requirement for a stable environment.

Here, we present a simple and easily accessible broadband spectroscopy scheme with hertz-level precision based on a tunable diode laser. The diode laser frequency is referenced on-the-fly by a high-finesse fiber cavity. The observant reader might notice that this referencing to a fiber cavity poses two problems: (1) the resonances of a fiber cavity are not equally spaced due to dispersion, and (2) the rate at which the tunable laser changes its frequency suffers from fluctuations, which makes it difficult to predict its frequency tuning into the future. We solve both of these problems by *in situ* calibration of the high-finesse fiber cavity mode spacing using sidebands modulated onto the tunable laser. As shown in Fig. 1(a), the resonances of a high-precision-calibrated dispersive cavity provide a series of frequency markers in time domain that are used to precisely determine the instantaneous frequency range of a CW laser while tuning its wavelength. A dual radio-frequency (RF) modulation scheme is used to calibrate the dispersive cavity on-the-fly with high precision, as shown in Fig. 1(b). Dual RF signals modulate the frequency of the tunable CW laser, which generates optical sidebands that are used to determine the cavity free spectral range (FSR). We apply this method to measure mode spectra of a fiber loop cavity with sub-10-Hz frequency resolution across an 11-THz spectral range within 10 s, revealing its complex dispersion profile. We use the calibrated cavity for several applications, including gas absorption spectroscopy and the measurement of mode spectra of integrated photonic devices, resulting in a relative precision across the 11-THz spectral range of 2×10^{-8}. This spectroscopy method enables a broad spectral range (limited by that of the tunable laser), fast measurement speed, ultrahigh frequency precision, and high optical power. The relatively simple setup makes this method very robust for out-of-the-lab applications. We believe it can become a powerful tool for high-precision broadband spectroscopy, lidar, environmental monitoring, and characterization of photonic devices.

2 Results

2.1 Schematic and Principle of the Hertz-level Broadband Spectrometer

Figure 1 illustrates the schematic and the working principle of a hertz-level broadband spectrometer based on dual RF modulation. As shown in Fig. 1(a), an external cavity diode laser with a widely tunable frequency range is modulated by two RF signals via an electro-optic intensity modulator (EOM), generating four optical sidebands in the frequency domain. The dual-RF modulated light is used to probe a reference cavity with an FSR smaller than or similar to the modulation frequency, such as fiber loop cavities, fiber linear cavities, and Fabry–Perot cavities. Important is only a high finesse and narrow linewidth of the reference cavity. Note that this reference cavity also exhibits dispersion, such that the FSR changes with wavelength. Depending on the FSR of the reference cavity, the frequency of the two RF signals f_{mod1}, f_{mod2} ($f_{\mathrm{mod1}} > f_{\mathrm{mod2}}$) can be set to around $(n + 1/2) \times \mathrm{FSR}$, where n is an integer number or zero. The frequency difference f_d between the two RF signals can be set to around a few megahertz, depending on the optical linewidth of the dispersive cavity. The transmitted or reflected light of the reference cavity is monitored by a photodiode (PD) and recorded by an oscilloscope. Figure 1(b) shows the principle of time-to-frequency conversion based on the dual RF modulation. As plotted in the frequency domain [upper part of Fig. 1(b)], we determine the moment in time (t_0) when the laser carrier frequency f_{carrier} is exactly in the middle between two reference cavity resonances, which are separated from each other by $(2n + 1) \times \mathrm{FSR}$. Just a tiny amount of time before t_0, the modulation sidebands (1) and (2) cross a cavity resonance, generating calibration markers (1) and (2) in the time domain. When the tunable laser continues sweeping toward higher frequencies, the modulation sidebands (3) and (4) will generate additional calibration markers. As a result, we measure four calibration marker transmission dips that are symmetric around t_0. These are used to determine the local FSR of the reference cavity with ultrahigh precision as well as the scan speed of the laser. In addition to the four calibration markers in the time domain, we also measure additional transmission dips when the tunable laser itself crosses the cavity resonances, as shown in the lower part of Fig. 1(b). This pattern repeats every time the tunable laser crosses one FSR of the reference cavity. An animation of this measurement scheme is available in the Supplementary Material. As shown in Fig. 1(b), the local FSR of the dispersive cavity is determined by $(2n + 1) \times \mathrm{FSR} = 2f_{\mathrm{mod1}} + f_?$ where $f_?/2$ is the frequency difference between the optical sideband f_{mod1} and nearby cavity resonance when the carrier frequency lies in the middle of two cavity resonances. Since we know f_{mod1} and n, we just need to determine $f_?$. From Fig. 1(b), we can see that the laser took the time interval $(t_3 - t_2)$ to scan across $f_?$. In addition, we know a precise value for the current laser scan speed, which is given by $v_{\mathrm{scan}} = f_d/(t_2 - t_1)$ or $v_{\mathrm{scan}} = f_d/(t_4 - t_3)$, where $f_d = f_{\mathrm{mod1}} - f_{\mathrm{mod2}}$ is the difference between the RF modulation frequencies. Thus, we obtain $f_? = v_{\mathrm{scan}} \times (t_3 - t_2)$. We can take the average of the two ways to calculate the scan speed v_{scan} to increase the measurement precision. Note that we can set the RF modulation frequencies close to each other, such that all the calibration markers 1–4 are recorded with little temporal offset. This allows us to achieve a nearly instantaneous calibration of the cavity FSR and the

current laser scan speed. Under this setting, the measurement is largely insensitive to fluctuations of the laser scan speed, which we assume to be constant within the tiny time interval $(t_3 - t_2)$. In comparison, for a single RF modulation scheme, the calculation of the laser scanning speed would involve averaging the scanning speed over a much longer time duration. During this period, the laser scans across $(n + 1/2) \times \mathrm{FSR}$. This would induce a relatively large frequency uncertainty in $f_?$. Details on the FSR calculation can be found in Note 1 in the Supplementary Material. As shown in Fig. 1(a), by utilizing the calibrated dispersive cavity and optionally incorporating an absolute frequency reference from atomic or molecular absorption lines, this spectroscopy method can be applied to measure integrated photonic devices like microresonators, for open-path gas sensing or generally optical frequency metrology. Notably, this approach is highly robust for out-of-lab applications, as it does not depend on mode-locked frequency combs or optical stabilization schemes, making it particularly advantageous for use in challenging or rough environments.

2.2 Characterization of the Fiber Loop Cavity

As a proof-of-concept demonstration, we verify our scheme by measuring the dispersion of a fiber loop cavity. The fiber cavity is made from a 10-dB fiber coupler and 5 m standard telecom fiber (SMF-28) with a zero-dispersion wavelength of 1310 nm. The FSR of the fiber cavity is 39 MHz, and the mode linewidth is 1 MHz, which limits the measurement speed to around 1 THz/s.[20] To demonstrate the ultrahigh frequency precision of our scheme, we use a 1.3-μm laser with a tuning range from 1270 to 1330 nm in order to resolve the small FSR variation of the fiber cavity around the zero-dispersion wavelength. In the experiment, the tunable laser is modulated by two 20-GHz signals with a 4-MHz frequency difference. The two RF signals are combined with a power combiner and applied to the EOM. The light transmitted through the fiber cavity is detected by a PD and recorded using an oscilloscope with a memory depth of 62.5 million data points. The frequency resolution is determined by the laser scanning speed (1 THz/s) and the oscilloscope sampling rate (5 MSa/s), resulting in a frequency resolution of 200 kHz.

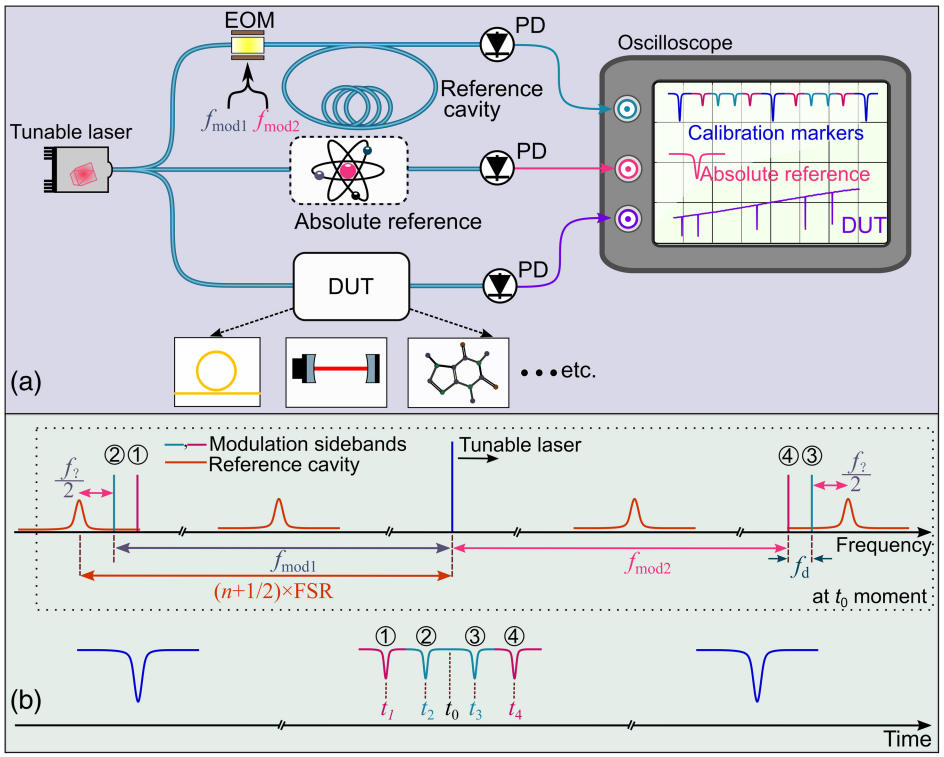

Fig. 1 Principle of a hertz-level broadband spectrometer based on dual RF modulation. (a) Measurement scheme. A tunable CW laser is modulated by two RF signals $(f_{\mathrm{mod1}}, f_{\mathrm{mod2}})$ via an EOM. The modulated light is used to probe a reference cavity with quasi-periodic structures, such as a fiber cavity or integrated photonic cavity. The transmitted light is monitored by a PD and recorded by an oscilloscope to provide frequency reference markers for the scanning diode laser. The referenced diode laser is used to spectrally measure devices under test, such as on-chip photonic devices or gas absorption spectra. Optionally, part of the light probes a narrow linewidth atomic/molecular transition for an absolute frequency reference. (b) Principle of time-to-frequency conversion based on dual RF modulation. Dual RF modulation generates two sidebands neighboring the carrier frequency on both sides plotted on the frequency axis. While scanning the laser frequency, the generated sidebands form four additional transmission dips together with the carrier transmission dips in the time domain. The laser scan speed, laser frequency, and FSR can be precisely traced back to the modulation frequencies and their difference, and the time interval between the small sideband dips.

This resolution is presently constrained by the memory depth of the oscilloscope utilized in our measurements, which limits the sampling rate to 5 MSa/s. However, using a more advanced oscilloscope with a memory depth of 3×10^9 points could elevate the sampling rate to 300 MSa/s, thereby achieving a frequency resolution of 3.3 kHz. In this case, the laser linewidth of 10 kHz would impose the ultimate limit on frequency resolution. The accuracy of the FSR measurement can be traced to that of the modulated RF signal, which is referenced to a rubidium clock with an accuracy of 5×10^{-11}.

Figure 2(a) shows the transmission spectrum of the fiber cavity from 1270 to 1330 nm; the inset shows an enlarged section of the data around 1300 nm. The deep transmission dips are fiber cavity resonances seen directly by the carrier, while the four additional small dips within one FSR result from the modulation sidebands crossing resonances. Figure 2(b) shows the measured FSR evolution of the fiber loop cavity as a function of wavelength around the zero-dispersion regime. The blue trace (upper panel) in Fig. 2(b) shows the results calculated from the dual RF modulation scheme. With a sub-10-Hz frequency precision, the blue trace clearly resolves the small FSR variation (<800 Hz) for a range of 11 THz and reveals the evolution of the cavity dispersion from normal at short wavelengths (FSR increasing with wavelength), crossing zero (region with nearly constant FSR), and to anomalous dispersion at longer wavelengths (FSR decreasing with wavelength). The black trace is the second-order polynomial fit with the zero-dispersion wavelength at 1315 nm. For comparison, the red trace (lower panel) in Fig. 2(b) shows the calculated FSR evolution based on a single RF modulation sideband (20 GHz modulation frequency), which cannot resolve the small changes of the cavity FSR. This demonstrates that our dual RF modulation, with ultrahigh precision in determining the laser scan speed and cavity FSR, is critical for the effectiveness of this spectroscopy method. Figure 2(c) shows the frequency difference of the measured FSRs by dual RF modulation with respect to the fitted values. Figure 2(d) shows a histogram of the frequency difference based on the data in Fig. 2(c), with a root-mean-square deviation of 8.3 Hz. To further verify our study, additional experiments are performed by using two independent 5-m fiber loop cavities (see Note 2 in the Supplementary Material for details).[31] These results confirm the ultrahigh-frequency precision of our dual RF broadband spectroscopy.

Figure 3(a) shows the calculated group velocity dispersion β_2 of the 5-m-long fiber cavity, based on the fitted data in Fig. 2(b). The results agree well with the dispersion of standard telecom fiber. The blue trace in Fig. 3(b) shows the corresponding group delay dispersion (GDD) of the 5-m-long fiber loop cavity, which includes the dispersion of a 10-dB coupler that is part of the cavity. We can use this setup to precisely measure dispersion of optical fibers by adding fiber to the cavity and measuring the change in dispersion. The red trace in Fig. 3(b) shows data

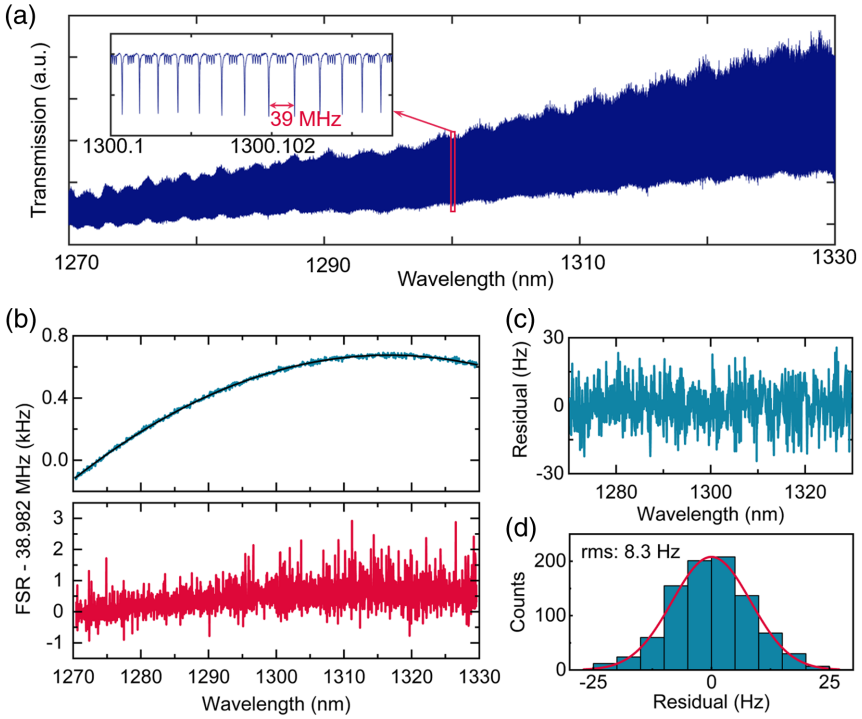

Fig. 2 Mode spectrum measurement of a fiber loop cavity calibrated by dual RF modulation. (a) Transmission spectrum of the 5-m fiber loop cavity. Inset, zoomed-in section showing the calibration markers around 1300 nm. The deep transmission dips are cavity resonances measured by the sweeping carrier laser while the small four dips within one FSR result from the RF modulation sidebands. (b) Measured FSR evolution (blue, upper panel) of the fiber loop cavity interrogated by the dual RF modulation scheme, together with a second-order polynomial fit (black), in contrast to the result (red, lower panel) measured by single RF modulation. (c) Frequency difference between the measured FSR by dual RF modulation and the fitted curve in panel (b). (d) Histogram of the data in panel (c) and a fitted Gaussian curve with an rms deviation of 8.3 Hz.

from another measurement with 3 m fiber removed from the cavity, leading to a 2-m-long cavity with a zero-dispersion wavelength of 1318 nm. By subtracting the GDD of the 2-m-long fiber cavity from that of the 5-m-long cavity, we can get the GDD of the removed 3-m-fiber, which is shown as a black trace in Fig. 3(b) with a zero-dispersion wavelength of 1312 nm. From the measurements, we can see that the zero-dispersion wavelength of longer cavities approaches that of the fiber used.

2.3 Characterizing an On-chip Optical Microresonator

Instead of measuring dispersion of optical fibers, our method can be easily applied to spectrally characterize the optical properties of different optical components, such as dispersion-engineered broadband mirrors and integrated photonic circuits. We show this by characterizing the transmission spectrum of an optical microresonator.[19] As shown in Fig. 1(a), one part of the tunable CW laser is modulated by two RFs and injected into the fiber cavity to generate precise reference markers that are recorded with an oscilloscope. This allows us to know the current frequency of the laser with high precision at any given time during the sweep. We can now use another part of the laser for spectroscopy by simultaneously measuring a test device and recording the transmission signal on another channel of an oscilloscope, as shown in Fig. 1(a). To demonstrate this technique, we use the resonance frequencies of the calibrated 5-m fiber cavity as frequency markers to measure the transmission spectrum of an in-house fabricated Si_3N_4 ring resonator. The Si_3N_4 resonator is made from a 750-nm Si_3N_4 thin film that is deposited onto a 3-μm SiO_2 intermediate layer on a silicon substrate via low-temperature reactive sputtering.[32,33] The Si_3N_4 microresonator used in the experiments has a diameter of 200 μm and a waveguide cross section of 1.8 μm × 750 nm. The resonator has an FSR of 231 GHz and an intrinsic optical quality factor of 3 million. The resonance frequencies of a mode family in a dispersive resonator can be described by a Taylor series as[34,35]

$$\omega_\mu = \omega_0 + D_1\mu + \frac{D_2}{2!}\mu^2 + \frac{D_3}{3!}\mu^3 + \frac{D_4}{4!}\mu^4 + \ldots = \omega_0 + D_1\mu + D_{\text{int}}(\mu), \quad (1)$$

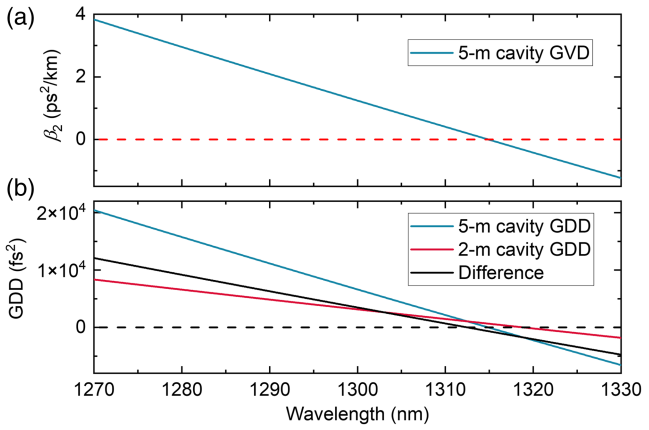

Fig. 3 Measured dispersion of the fiber cavity based on the fitted trace in Fig. 2(b). (a) Group velocity dispersion of a 5-m fiber cavity. (b) GDD of a 5-m-long fiber cavity (blue), 2-m-long fiber cavity (red), and 3 m of optical fiber.

where μ is the mode number offset from the center mode at $\mu = 0$ and ω_μ are the resonance frequencies. $D_1/2\pi$ is the FSR of the resonator at an arbitrarily chosen central mode ($\mu = 0$), and D_2, D_3, and D_4 are coefficients of second-, third-, and fourth-order dispersion, respectively. D_{int} is the integrated dispersion, depicting the deviation of resonance frequencies from the equidistant grid spaced by D_1. While scanning the frequency of the CW laser, both transmission signals from the fiber cavity and Si_3N_4 resonator are simultaneously recorded. Figure 4(a) shows the normalized transmission spectrum of the Si_3N_4 resonator. Two different mode families are observed. The red markers highlight the fundamental TE mode family. Figure 4(b) shows one microresonator resonance (blue) around 1270.6 nm together with frequency markers (red) from the fiber cavity. The inset in Fig. 4(b) shows a scanning electron microscope image of the resonator.

For such measurements, a referenced scanning across multiple FSRs of the reference cavity is used to determine the microresonator mode spacing. The same applies to the measurement of the spacing between hydrogen fluoride (HF) gas absorption lines, which will be shown later. This raises a question: Does the FSR error of the reference cavity accumulate linearly with the number of FSRs, thus degrading the measurement precision when increasing the laser frequency tuning range? In our measurement, we find that this is not the case, since the FSR of the reference cavity versus wavelength is fitted by a polynomial, and the fitted FSR values are used to determine the frequency distance between features under test. To experimentally validate this claim, we employ two independent 5-m fiber cavities to calibrate the frequency scanning of the tunable laser. The transmission of the two fiber cavities is recorded and used to convert the laser sweeping time to the optical frequency offset based on the FSR of each cavity independently. The obtained laser frequencies based on the two independent cavities are compared against each other, and the result shows excellent agreement with an rms value of 220 kHz for a scan from 1270 to 1330 nm. This rms frequency difference remains constant independent of the scan range. Thus, we achieve a relative precision of 2.0×10^{-8} for a frequency range of 11 THz, which is limited by the maximum tuning range of the laser used in the experiments. This surpasses existing tunable diode laser spectroscopy methods[15–20,36] by 2 orders of magnitude (see Note 2 in the Supplementary Material for details).

The *in situ* measured FSR of the fiber cavity and the corresponding reference markers are used to convert the time axis of the oscilloscope into optical frequencies. This allows us to measure the mode structure of the Si_3N_4 resonator, including the evolution of its mode spacing, resonance linewidth, and dispersion. Figure 4(c) shows the measured integrated dispersion profile (blue circles) at a central mode at 1310 nm together with a second-order polynomial fit (red), depicting the deviation of resonance frequencies from the equidistant grid spaced by the FSR at the central mode, based on the resonances with red markers in Fig. 4(a). The dispersion profile exhibits anomalous dispersion with mode crossings at 1280 and 1326 nm.[37] To verify the dispersion measurement, we test this Si_3N_4 resonator for the generation of a soliton frequency comb by pumping an optical mode at 1310 nm.[38,39] Figure 4(d) shows the optical spectrum of a single bright soliton with a fitted sech^2 envelope (blue dashed line),[39,40] which further verifies the anomalous dispersion regime for the pump mode. In addition, the mode crossing at 1326 nm in Fig. 4(c)

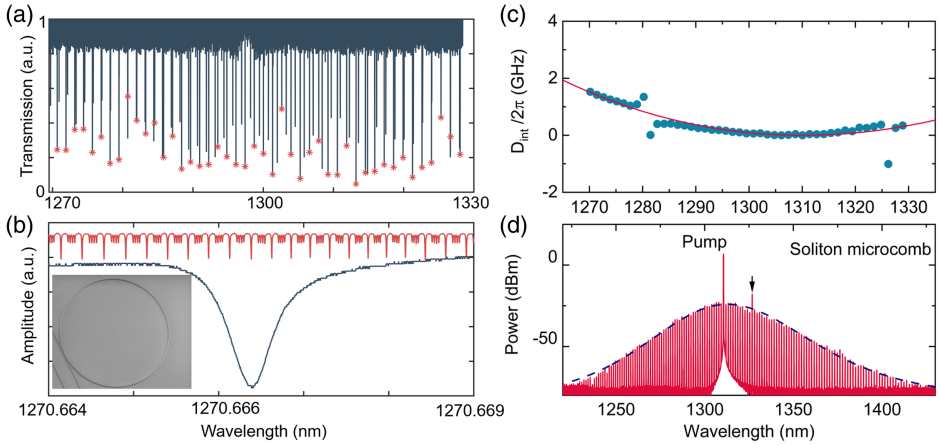

Fig. 4 Si_3N_4 resonator mode spectrum and dispersion measurement. (a) Normalized transmission spectrum of the Si_3N_4 on-chip resonator with red markers on the fundamental TE mode family. (b) Zoomed-in spectrum around 1270.6 nm together with fiber cavity resonance markers. Inset, scanning electron microscope image of the 200-μm-diameter Si_3N_4 resonator used in the experiments. (c) Measured integrated dispersion profile (blue circles) at pump wavelength of 1310 nm together with a second-order polynomial fit (red trace). (d) Optical spectrum of a bright soliton generated in the Si_3N_4 resonator pumped at 1310 nm and a sech^2 envelope fit (blue dashed trace). A dispersive wave (marked with an arrow) is observed at 1326 nm.

induces a dispersive wave (marked with an arrow) at 1326 nm in Fig. 4(d).[34]

2.4 Hydrogen Fluoride Gas Spectroscopy

To highlight another application of this spectroscopy method, we demonstrate the measurement of nonperiodic spectra, such as the absorption spectrum of a gas. A fiber-coupled HF gas cell with 50-Torr pressure and 2.7-cm optical path length is used for this demonstration. Just as before, the output light of the sweeping 1.3-μm CW laser is split into two paths; one part is referenced to the 5-m fiber cavity to generate calibration markers, while the other part is used for simultaneously probing the absorption spectrum of the gas cell. Figure 5(a) shows the strong HF molecular absorption lines (P and R branches) in the O-band range. Figure 5(b) shows the zoomed-in spectrum of the P(2) absorption line (solid black line) with fiber resonances (blue line) as frequency references. A Voigt function [dashed red line in Fig. 5(b)] is used to fit the spectral profile. For the fit, we use the calculated Gaussian full width at half-maximum (FWHM) linewidth (631.0 ± 0.2 MHz) based on the Doppler broadening.[41,42] The maximum transmission through the HF cell has been normalized to one. The corresponding fit residuals are less than 0.01 across the fitting range, as shown in Fig. 5(c). The fitted Lorentzian FWHM linewidth, including pressure broadening, is ~3150 MHz, which is higher than the value from high-resolution transmission molecular absorption database (HITRAN). This discrepancy is attributed to a slightly higher than specified gas pressure in the cell. Table 1 shows the measured position of the HF absorption lines in comparison to the HITRAN database.[43] Column 2 is the absorption line position calculated from the HITRAN database, corrected with the pressure shift from the vacuum transition wavelength. Columns 3 and 4 are the theoretically calculated Gaussian and Lorentzian FWHM linewidths, respectively. The uncertainty in the Lorentzian FWHM linewidth is calculated based on 20% uncertainty of the gas pressure, as specified by the gas cell manufacturer. The Gaussian linewidth and its uncertainty are calculated at a temperature of (21 ± 0.2)°C. Column 5 shows the measured line positions. Here, we use the measured R(2) line as absolute frequency reference and set its frequency equal to the value calculated from the HITRAN database.

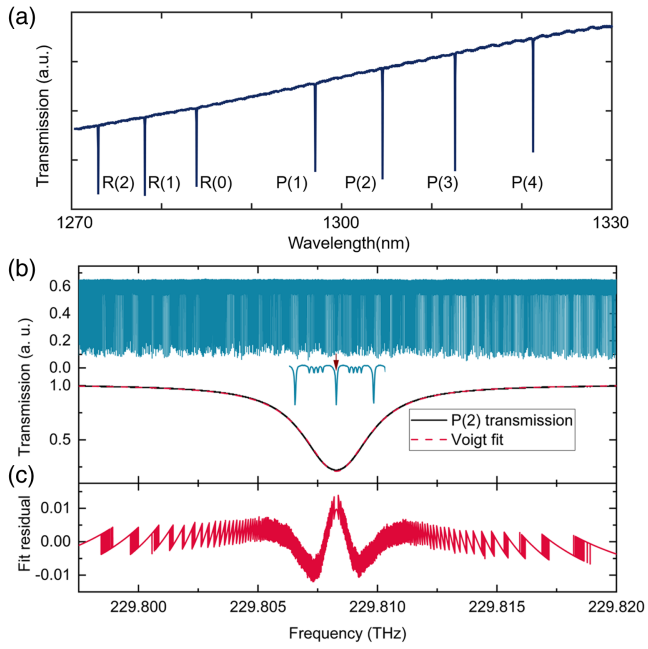

Fig. 5 Absorption spectrum of a gas cell filled with HF. (a) Transmission spectrum of the HF gas cell between 1270 and 1330 nm. (b) Spectral profile (solid black line) of the HF P(2) line together with the frequency markers (blue) from the 5-m fiber cavity. The dashed red line is a Voigt fit. (c) Fit residuals of the HF P(2) absorption line. The jumps in the fit residual are due to the discrete voltage resolution of the oscilloscope.

Table 1 Measured wavelengths and linewidth of HF absorption lines and comparison with values from the HITRAN database.

Line	HITRAN[a,b] (nm)	Cal. Gauss.[c] Δf (MHz)	Cal. Lorentz.[b] Δf (MHz)	Measured position[d] (nm)	Δ (pm)	Measured Lorentz. Δf (MHz)
R(2)	1272.97025 (±0.04 pm)	646.6 (±0.2)	2453.6 (±491.1)	1272.97025	—	3247 (±5)
R(1)	1278.14783 (±0.04 pm)	644.0 (±0.2)	2496.9 (±499.7)	1278.14751 (±0.02 pm)	−0.32	3281 (±7)
R(0)	1283.88526 (±0.09 pm)	641.1 (±0.2)	2260.3 (±452.4)	1283.88462 (±0.02 pm)	−0.64	2602 (±7)
P(1)	1297.07013 (±0.03 pm)	634.6 (±0.2)	2469.3 (±494.2)	1297.06915 (±0.02 pm)	−0.98	2689 (±5)
P(2)	1304.53367 (±0.04 pm)	631.0 (±0.2)	2741.5 (±548.7)	1304.53290 (±0.02 pm)	−0.77	3152 (±11)
P(3)	1312.59095 (±0.02 pm)	627.1 (±0.2)	2650.8 (±530.5)	1312.59057 (±0.03 pm)	−0.38	2827 (±11)
P(4)	1321.25259 (±0.02 pm)	623.0 (±0.2)	2039.4 (±407.9)	1321.25214 (±0.02 pm)	−0.45	2036 (±9)

[a]Data from HITRAN are given after adding a 50-Torr pressure shift.
[b]The uncertainties of the pressure shift and pressure-broadened linewidths are calculated from the pressure uncertainty of 20%.
[c]The temperature of the gas cell is 21°C ± 0.2°C.
[d]The measured R(2) wavelength is set equal to the value from HITRAN and used as an absolute reference.

The measurement uncertainty of 0.02 pm is calculated based on statistical analysis of multiple measurements acquired over a month. More details on the measurement uncertainty can be found in the Note 3 in the Supplementary Material. Column 6 is the wavelength difference between the measured results and the HITRAN database, showing that the measured line positions are at slightly shorter wavelengths than the calculated ones. Using the calculated Gaussian linewidth in column 3 and the Voigt fitting function, the last column shows the measured Lorentzian FWHM of the absorption lines. Considering that the measured Lorentzian (pressure broadened) linewidth is larger than the calculated numbers, we speculate that the pressure of the HF gas cell used in the experiments is higher than the 50 Torr specified by the manufacturer. The linewidth measurement of the absorption lines is verified through a modulation sideband spectroscopy technique. In this measurement, we modulate 10 GHz sidebands onto the tunable laser with an EOM. Then the laser with the modulation sidebands is scanned across each individual HF resonance. In the measurement, each HF resonance is recorded 3 times: one time by the laser and one time by each modulation sideband. To determine the Lorentzian FWHM linewidth of each absorption line, we use the known 10 GHz spacing between the measured absorption lines as reference. More details can be found in Note 4 in the Supplementary Material.

3 Conclusion

In summary, we have proposed and demonstrated a powerful broadband spectroscopy technique based on a tunable CW laser that overcomes the limitations of existing tunable diode laser spectroscopy with unprecedented precision. The laser frequency tuning is on-the-fly calibrated using a fiber cavity and a dual RF frequency modulation technique that precisely determines the laser scan speed and provides calibration markers. By combining the frequency accuracy of RF modulation sidebands with the short-term stability of a high-finesse fiber cavity, we realize a broadband and easy-to-use optical frequency ruler for determining frequency distances between features under test with ultrahigh precision. Applying this method, we can measure miniscule FSR deviations of a fiber loop cavity at close-to-zero dispersion over an 11-THz frequency range on-the-fly with sub-10-Hz precision, which is an improvement of 1 order of magnitude in comparison with existing tunable laser spectroscopy methods.[15,19,44,45] The demonstrated measurement speed is 1 THz/s, which was limited by the cavity linewidth of the corresponding reference cavity buildup time. Compared to frequency comb-based spectroscopy, this scheme provides high optical probe power as well as better spectral flatness and polarization stability. In addition, this method could enable access to new wavelength regions, e.g., in the mid-infrared or UV. We demonstrate several applications by characterizing the dispersion of an integrated photonic microresonator and measuring the molecular absorption spectrum of HF gas with a 2-orders-of-magnitude improvement in precision compared to existing tunable laser spectroscopy methods.[15–20,36] Using a well-known atomic/molecular transition or a characteristic gas absorption fingerprint as absolute frequency reference, this method can be used for highly accurate broadband molecular spectroscopy,[46] providing a microwave link between optical frequencies. In addition, without the requirement of mode locking or phase locking, this simple and robust method can find applications in out-of-the-lab settings where extremely high absolute accuracy is not required. These applications include lidar systems,[24] 3D imaging,[28] refractive index measurements,[47] open-path trace-gas sources sensing,[48–50] characterization of photonic devices,[34,51] and calibration of astrophysical spectrometers.[52]

4 Appendix: Supplementary Video

Video 1: Animation of the principle of a hertz-level broadband spectrometer based on dual RF modulation (MP4, 1.55 MB [URL: https://doi.org/10.1117/1.AP.6.4.046003.s1]).

Disclosures

The authors filed a patent application for the demonstrated spectroscopy method.

Code and Data Availability

The data that support the findings of this study are available from the corresponding author upon reasonable request.

Acknowledgments

This work is supported by European Union's H2020 ERC Starting Grant "CounterLight" (Grant No. 756966), H2020 Marie Sklodowska-Curie COFUND "Multiply" (Grant No. 713694),

Marie Curie Innovative Training Network "Microcombs" (Grant No. 812818), and the Max Planck Society. S.Z. conceived and performed the experiments. S.Z., T.B., and P.D. analyzed the data. All co-authors contributed to the paper.

References

1. K. Shimoda, "Introduction," in *High-Resolution Laser Spectroscopy*, K. Shimoda, Ed., pp. 1–10, Springer, Berlin, Heidelberg (1976).
2. D. J. Jones et al., "Carrier-envelope phase control of femtosecond mode-locked lasers and direct optical frequency synthesis," *Science* **288**, 635–639 (2000).
3. R. Holzwarth et al., "Optical frequency synthesizer for precision spectroscopy," *Phys. Rev. Lett.* **85**, 2264–2267 (2000).
4. S. A. Diddams, K. Vahala, and T. Udem, "Optical frequency combs: coherently uniting the electromagnetic spectrum," *Science* **369**, eaay3676 (2020).
5. M. Takamoto et al., "Test of general relativity by a pair of transportable optical lattice clocks," *Nat. Photonics* **14**, 411–415 (2020).
6. N. Picqué and T. W. Hänsch, "Frequency comb spectroscopy," *Nat. Photonics* **13**, 146–157 (2019).
7. T. Fortier and E. Baumann, "20 years of developments in optical frequency comb technology and applications," *Commun. Phys.* **2**, 153 (2019).
8. A. Marian et al., "United time-frequency spectroscopy for dynamics and global structure," *Science* **306**, 2063–2068 (2004).
9. F. Keilmann, C. Gohle, and R. Holzwarth, "Time-domain mid-infrared frequency-comb spectrometer," *Opt. Lett.* **29**, 1542–1544 (2004).
10. I. Coddington, N. Newbury, and W. Swann, "Dual-comb spectroscopy," *Optica* **3**, 414–426 (2016).
11. S. A. Diddams, L. Hollberg, and V. Mbele, "Molecular fingerprinting with the resolved modes of a femtosecond laser frequency comb," *Nature* **445**, 627–630 (2007).
12. J. Mandon, G. Guelachvili, and N. Picqué, "Fourier transform spectroscopy with a laser frequency comb," *Nat. Photonics* **3**, 99–102 (2009).
13. Q.-F. Yang et al., "Vernier spectrometer using counterpropagating soliton microcombs," *Science* **363**, 965–968 (2019).
14. S. Pan and M. Xue, "Ultrahigh-resolution optical vector analysis based on optical single-sideband modulation," *J. Lightwave Technol.* **35**, 836–845 (2017).
15. Y.-H. Luo et al., "A wideband, high-resolution vector spectrum analyzer for integrated photonics," *Light Sci. Appl.* **13**, 83 (2024).
16. D. K. Gifford et al., "Optical vector network analyzer for single-scan measurements of loss, group delay, and polarization mode dispersion," *Appl. Opt.* **44**, 7282–7286 (2005).
17. S. Fujii and T. Tanabe, "Dispersion engineering and measurement of whispering gallery mode microresonator for Kerr frequency comb generation," *Nanophotonics* **9**, 1087–1104 (2020).
18. C. Jin et al., "High-resolution optical spectrum characterization using optical channel estimation and spectrum stitching technique," *Opt. Lett.* **38**, 2314–2316 (2013).
19. J. Li et al., "Sideband spectroscopy and dispersion measurement in microcavities," *Opt. Express* **20**, 26337–26344 (2012).
20. P. Del'Haye et al., "Frequency comb assisted diode laser spectroscopy for measurement of microcavity dispersion," *Nat. Photonics* **3**, 529–533 (2009).
21. T. Qing et al., "Optical vector analysis with attometer resolution, 90-dB dynamic range and THz bandwidth," *Nat. Commun.* **10**, 5135 (2019).
22. J. Liu et al., "Frequency-comb-assisted broadband precision spectroscopy with cascaded diode lasers," *Opt. Lett.* **41**, 3134–3137 (2016).
23. K. Twayana et al., "Frequency-comb-calibrated swept-wavelength interferometry," *Opt. Express* **29**, 24363–24372 (2021).
24. E. Baumann et al., "Comb-calibrated frequency-modulated continuous-wave ladar for absolute distance measurements," *Opt. Lett.* **38**, 2026–2028 (2013).
25. W. Yu et al., "Comb-calibrated frequency sweeping interferometry for absolute distance and vibration measurement," *Opt. Lett.* **44**, 5069–5072 (2019).
26. F. R. Giorgetta et al., "Fast high-resolution spectroscopy of dynamic continuous-wave laser sources," *Nat. Photonics* **4**, 853–857 (2010).
27. K. Knabe et al., "Frequency characterization of a swept- and fixed-wavelength external-cavity quantum cascade laser by use of a frequency comb," *Opt. Express* **20**, 12432–12442 (2012).
28. E. Baumann et al., "Comb-calibrated laser ranging for three-dimensional surface profiling with micrometer-level precision at a distance," *Opt. Express* **22**, 24914–24928 (2014).
29. A. Nishiyama, D. Ishikawa, and M. Misono, "High resolution molecular spectroscopic system assisted by an optical frequency comb," *J. Opt. Soc. Am. B* **30**, 2107–2112 (2013).
30. C. Fredrick et al., "Thermal-light heterodyne spectroscopy with frequency comb calibration," *Optica* **9**, 221–230 (2022).
31. M. Ding et al., "Optical fiber delay lines in microwave photonics: sensitivity to temperature and means to reduce it," *J. Lightwave Technol.* **39**, 2311–2318 (2021).
32. A. Frigg et al., "Low loss CMOS-compatible silicon nitride photonics utilizing reactive sputtered thin films," *Opt. Express* **27**, 37795–37805 (2019).
33. S. Zhang et al., "Low-temperature sputtered ultralow-loss silicon nitride for hybrid photonic integration," *Laser Photonics Rev.* **18**, 2300642 (2024).
34. V. Brasch et al., "Photonic chip–based optical frequency comb using soliton Cherenkov radiation," *Science* **351**, 357–360 (2016).
35. S. Zhang et al., "Spectral extension and synchronization of microcombs in a single microresonator," *Nat. Commun.* **11**, 6384 (2020).
36. Z. Tang, S. Pan, and J. Yao, "A high resolution optical vector network analyzer based on a wideband and wavelength-tunable optical single-sideband modulator," *Opt. Express* **20**, 6555–6560 (2012).
37. T. Herr et al., "Mode spectrum and temporal soliton formation in optical microresonators," *Phys. Rev. Lett.* **113**, 123901 (2014).
38. P. Del'Haye et al., "Optical frequency comb generation from a monolithic microresonator," *Nature* **450**, 1214–1217 (2007).
39. T. Herr et al., "Temporal solitons in optical microresonators," *Nat. Photonics* **8**, 145–152 (2014).
40. S. Zhang et al., "Sub-milliwatt-level microresonator solitons with extended access range using an auxiliary laser," *Optica* **6**, 206–212 (2019).
41. G. Guelachvili, "Absolute wavenumber measurements of 1-0, 2-0, HF and 2-0, $H^{35}Cl$, $H^{37}Cl$ absorption bands," *Opt. Commun.* **19**, 150–154 (1976).
42. G. Guelachvili and M. A. H. Smith, "Measurements of pressure-induced shifts in the 1-0 and 2-0 bands of HF and in the 2-0 bands of $H^{35}Cl$ and $H^{37}Cl$," *J. Quantum Spectrosc. Radiat. Transf.* **20**, 35–47 (1978).
43. I. E. Gordon et al., "The HITRAN2016 molecular spectroscopic database," *J. Quantum Spectrosc. Radiat. Transf.* **203**, 3–69 (2017).
44. N. Y. Dmitriev et al., "Measurement of dispersion characteristics of integrated optical microresonators and generation of coherent optical frequency combs," *J. Exp. Theor. Phys.* **135**, 9–19 (2022).
45. Z. He et al., "Simple and accurate dispersion measurement of GaN microresonators with a fiber ring," *Opt. Lett.* **48**, 2182–2185 (2023).
46. A. Shkarin et al., "Nanoscopic charge fluctuations in a gallium phosphide waveguide measured by single molecules," *Phys. Rev. Lett.* **126**, 133602 (2021).
47. L. Yang et al., "Frequency comb calibrated frequency-sweeping interferometry for absolute group refractive index measurement of air," *Appl. Opt.* **56**, 3109–3115 (2017).

48. D. I. Herman et al., "Precise multispecies agricultural gas flux determined using broadband open-path dual-comb spectroscopy," *Sci. Adv.* **7**, eabe9765 (2021).
49. G. B. Rieker et al., "Frequency-comb-based remote sensing of greenhouse gases over kilometer air paths," *Optica* **1**, 290–298 (2014).
50. S. Coburn et al., "Regional trace-gas source attribution using a field-deployed dual frequency comb spectrometer," *Optica* **5**, 320–327 (2018).
51. A. Nishiyama, A. Matsuba, and M. Misono, "Precise frequency measurement and characterization of a continuous scanning single-mode laser with an optical frequency comb," *Opt. Lett.* **39**, 4923–4926 (2014).
52. S. Minardi, R. J. Harris, and L. Labadie, "Astrophotonics: astronomy and modern optics," *Astron. Astrophys. Rev.* **29**, 6 (2021).

Shuangyou Zhang is a senior scientist at the Max Planck Institute for the Science of Light. He received his BS degree in electronics from Jilin University in 2010 and his PhD in electronics from Peking University in 2016. He is the author of more than 40 journal papers and has written one book chapter. His current research interests include integrated photonics, optical frequency combs and their applications, chip-scale atomic clock, and two-photon-transition for optical frequency standards.

Toby Bi is currently pursuing his Dr. rer. nat degree within the Microphotonics Research Group at the Max Planck Institute for the Science of Light and at Friedrich-Alexander Universität Erlangen-Nürnberg. Between 2020 and 2023, he was involved with the Marie Skłodowska-Curie Innovative Training Network Microcombs. He obtained his BSc degree with honors and his MSc degree from the University of Auckland, New Zealand, in 2017 and 2019, respectively. His research interests are focused on nonlinear optics and integrated photonics.

Pascal Del'Haye is heading the Microphotonics Research Group at the Max Planck Institute for the Science of Light since 2020. He is an expert on integrated photonics, microresonator-based frequency combs, and nonlinear optics. After graduating at LMU Munich, he worked at NIST, Boulder, Colorado, United States and the National Physical Laboratory in the United Kingdom. His scientific work on metrology, integrated photonics, and nonlinear optics has been cited more than 10,000 times, and he has received numerous awards and prizes, including the Helmholtz Prize for Metrology and the EFTF Young Scientist Award.